Modelling the morphodynamic evolution of Galveston beach, Gulf of Mexico, following Hurricane Ike in 2008

Antonios Valsamidis[a], Jens Figlus[b], Benjamin Ritt[c], Dominic E Reeve[a,*]

[a]College of Engineering, Bay Campus, Swansea University, Swansea, SA1 8EN, UK

[b]The Department of Ocean Engineering, College of Engineering, Texas A&M University, Galveston Campus, Galveston, TX 77554, USA.

[c]The Department of Marine Sciences, Texas A&M University, Galveston Campus, Galveston, TX 77554, USA.

* Corresponding author. E-mail address: d.e.reeve@swansea.ac.uk (D.E. Reeve)

Abstract

A unique set of field measurements taken along Galveston beach have been compiled to give annual shoreline positions over the period 2010-2016. These have been used, in conjunction with statistical and mathematical modelling, to gain insights into the response of the shoreline after the landfall of Hurricane Ike in 2008, which caused extensive erosion and loss of material from the beach. Over the period 2010-2014, a generally accretive trend is observed along the beach. Within this trend, two different patterns are evident. In the area extending westward of South Jetty the accretion rate is fast until April 2011, after which the accretion rate decreases. The remainder of the beach, including the groyne field in front of the city of Galveston, exhibits the greatest accretive trend after April 2011. It is hypothesised that distinct sandbanks lying offshore of Galveston Island were formed during the passage of Hurricane Ike and control these two different patterns of recovery. To test this hypothesis a novel 1-line model, based on linked analytical solutions, was set up to investigate the beach response to various sediment source distributions. The model was tested against existing

survey measurements and performed satisfactorily. An exploration of various sediment supply scenarios with the model supports the hypothesis that offshore sediment stores, one distinct source to the south of South Jetty and a diffuse linear source running the length of the groyne field and seawall, were gradually being fed back to the beach by the prevailing wave conditions.

Keywords: groyne-field, shoreline evolution, accretion, One-Line model, Galveston beach, Hurricane Ike, semi-analytical solution

1. Introduction

1.1. Background

Galveston Island is a sandy barrier island system near Houston in the Gulf of Mexico that extends *44 km* alongside the mainland, from Bolivar Roads to San Luis Pass (Fig. 1). A unique set of shoreline surveys has provided the basis for an exploration of the recovery of Galveston beach after the passage of Hurricane Ike. These, combined with a semi-analytical one-line model, have been used to gain insights into the meso-scale recovery process of the beach. An explanation of the morphodynamic evolution of a section of Galveston beach near Galveston city extending approximately 17km westwards from South Jetty is proposed, as a result.

Shoreline changes and sediment budgets in this area are affected by natural processes. Two inlets, namely Bolivar Roads and San Luis Pass, and engineered coastal structures including jetties, the Galveston seawall, and an associated groyne field in front of the seawall act to control the sediment movement along the shore. Bolivar Roads is the main ship channel connecting the Gulf of Mexico and Galveston Bay enabling ship traffic in and out of several major harbours (Houston, Galveston, Texas City). The shipping lane is maintained to a depth of *14 m* and is protected by jetties on either side. The north and south jetties extend *7.6* and

3.9 km, respectively, from the shoreline. San Luis Pass is an inlet not maintained by dredging but with notable sediment movements related to its banks and shoals. The seawall was constructed after the devastating hurricane that occurred in 1900, and extends approximately 16 km from the South Jetty to the southwest direction, and its height is 5 to 6m (Doran et al., 2009), providing protection from storm surge and wave action mainly to the city of Galveston. In the middle of the 20th century 15 groynes were constructed to maintain the sandy beach, both for recreational purposes and as scour protection for the seawall. The direction of net longshore sediment transport along most of the northern and central Texas coastline is to the southwest (Hall, 1976; Mason, 1981) but a divergent nodal zone (reversal in net direction) is present in the vicinity of the western portion of Galveston seawall. East of this region net sediment transport is in a northeasterly direction toward South Jetty and the entrance of the Bolivar Roads ship channel (King, 2007; Morang, 2006), whereas west of the nodal zone net transport is directed toward the west end of Galveston Island and San Luis Pass (Frey et al., 2014), as indicated in Fig. 1.

Fig. 1.

1.2. Post-storm beach recovery

Following beach erosion that may be caused in Galveston island by storm events, the natural process of beach recovery takes place. Generally, beach recovery is a composite phenomenon affecting the whole beach profile from the lower shoreface and nearshore to the coastline, the backshore, and dunes. Different natural mechanisms dominate beach recovery in different parts of a beach, for instance, wave shoaling may cause sediment deposits which had previously been placed in the lower shoreface to move back towards the shore (Hallermeier,

1980, Nielsen and Lord, 1993), while aeolian processes act as the primary restoring force of eroded backshore and dunes (e.g. McLean and Shen, 2006; Houser and Mathew, 2011). Although the storm effects on beach morphodynamics have been studied in detail (e.g., Larson and Kraus, 1989; Roelvink et al., 2009) beach recovery processes have not yet been investigated adequately (Jensen et al., 2009; Corbella and Stretch, 2012). Beach recovery is characterized by some factors such as the tidal range in a specific site and the corresponding modal wave energy (Phillips, 2018); the first refers to tidal currents that potentially push back sediment material towards the shore, that was previously driven offshore-wards due to storm forcing, while the second one to the available wave energy in a coastal site that may mobilize sediment materials deposited offshore, towards the upper beach. The aforementioned characteristics, as well as other site specific quantities such as the grain size of the beach material, determine the duration of beach recovery which can vary from few months to several years (e.g. Kobayashi and Jung, 2012; Philips et al., 2015). Recovery can be longer still; for instance Flemming and Davis (1994) reported that the shoreline at Spiekeroog Island near northern Holland exhibits beach recovery after storm erosion over a period of 11 to 14 years.

Galveston beach is characterized by low wave energy (Short and Woodroffe, 2009) and is a microtidal one (Davies, 1980) as it is located in the Gulf of Mexico. Following a storm event, the observed recovery duration of the Galveston shoreline and berm varies from few months to one year (Morton et al., 1994), while the corresponding recovery duration of the backshore and dune is about four to five years (Morton and Paine, 1985; Morton et al., 1994). However, Hurricane Ike which made a landfall in Galveston Island in 2008 caused a prolonged shoreline recovery process which took many years to be completed as will be shown in the following sections of this study. Therefore, Galveston beach was investigated aiming at

99 understanding the underlying physical mechanisms of its morphodynamic evolution
100 following Hurricane Ike in 2008.
101
102 **2. The study area**
103 Nearshore geological surveys around Galveston Island have indicated that longshore
104 transport rates of 115,000 m^3/yr are typical, (having been of this order for several millennia),
105 and that washover rates are negligible, (Wallace et al. 2010). The Galveston coastal region is
106 quite limited in terms of sediment supply from rivers. Specifically, most sandy material
107 carried by the Trinity River is deposited in Lake Livingston (Phillips and Musselman, 2003)
108 and sediment from the lower Trinity River is accommodated within the delta in Trinity Bay
109 (Phillips et al., 2004) and does not reach the Gulf of Mexico shoreline. The Brazos River to
110 the southwest of Follet's Island, the island adjacent to Galveston, carries a much reduced
111 sediment load due to damming (Dunne and Raines, 2001), and in addition, its mouth has been
112 relocated further west in an effort to reduce maintenance on the Freeport harbour entrance
113 (Kraus and Lin, 2002). Fig. 2 summarizes the geographical configuration of the main
114 locations and key features.
115
116 Fig. 2.
117
118 Evidence presented by King (2007) suggests that sand present in the Bolivar Roads ship
119 channel, along the Gulf of Mexico beaches and in the surf zone of Galveston Island is either
120 reworked from relic deposits or remains within the shoreline as it retreated landward at the
121 end of the last ice age. This leaves the coastal zone in the area sand-limited, consisting only
122 of a thin sand veneer perched on a mud substrate, with minimal new supply entering the
123 system (Frey et al., 2014). The latter might come from Galveston Entrance Channel which is

regularly dredged by the USACE with the intention of maintaining the navigation channel, with the dredged material deposited in the vicinity of the seaward tip of South Jetty. Sediment transport along the Gulf coast shoreline is driven by wave-induced nearshore currents and depends heavily on the complex offshore bathymetry which modifies approaching wave fields through refraction and diffraction. Therefore, it is not surprising that an erosional trend has been observed over time along most of the Galveston beaches while accretion has occurred on both ends of Galveston. Specifically, the unprotected shoreline between the western tip of the seawall and San Luis Pass (Fig. 1) was found to be retreating at moderate rates between *0.6* to *2.0 m/yr* with some portions of Galveston's west end near the western end of the seawall retreating at rates higher than *2.0 m/yr*, while stretches protected by the seawall were considered stable, in part due to occasional nourishment efforts, (Paine et al., 2011; Gibeaut, 2011). Both ends of Galveston Island and the western end of the Bolivar Peninsula have been observed to accrete at rates of up to *5 m/yr* (Paine, 2011).

The sediment in the nearshore zone is made up of sand (84 %) and fines (16 %). The coastal sand residing in the system is very fine with a median diameter D_{50} around *0.15 mm* (Frey et al., 2014). Offshore sediments outside the active surf zone along the coastline are largely mud-dominated but some limited pockets of beach quality sand exist (White et al., 1985; Siringan and Anderson, 1994; Anderson and Wellner, 2002; Finkl et al., 2004; Williams et al., 2012). Offshore beach quality sand is contained mainly in features like Heald Bank (55 km offshore) or Sabine Bank (110 km offshore) with an estimated 585 million cubic metres and 1.2 billion cubic metres of material, respectively (Morton et al., 1994).

Hurricane Ike made landfall at the eastern part of Galveston Island (Hawkes and Horton, 2012) over the western part of Bolivar Peninsula (Sherman et al., 2013), as an extreme Category 2 hurricane on the 13th of September 2008. Hurricane Ike passed through Galveston

149 Bay leaving Houston to its left side while propagating further onto the mainland (Hawkes and
150 Horton 2012). The path of Hurricane Ike was tracked by Rego and Li (2010) and Sherman et
151 al. (2013), and shown in Figure 3.
152
153 Fig. 3.
154
155 Extreme events such as hurricanes can have a significant effect on sediment budgets by
156 transporting large volumes of sediment onshore into the bay (barrier island rollover) or
157 offshore via shore face erosion or surge ebb flow (e.g., Sallenger, 2000; Morton et al., 2003;
158 Houser et al., 2008). Goff et al. (2010) showed that storm surge ebb flows across the Bolivar
159 Peninsula, near Galveston Island, moved sediment far enough offshore during Hurricane Ike
160 that they were lost to the beach and barrier system.
161 The unprotected part of Galveston Island, west of the seawall, is comprised of sandy beaches
162 with dunes rising about 2 to 4 m above sea level. This area suffered the erosive impacts of
163 Hurricane Ike to a greater degree than the region protected by the seawall and the groyne
164 field, although the sandy beach in front of the seawall also experienced significant erosion,
165 (Doran et al., 2009). Fig. 4 illustrates erosion caused by Hurricane Ike in front of the seawall
166 and the groyne field (Fig. 4a and 4b), and near South Jetty (Fig. 4c and 4d).
167
168 Fig. 4.
169
170 In the aftermath of Hurricane Ike bathymetric surveys were commissioned by the Galveston
171 Park Board of Trustees over the period 2010-2016. For the purposes of this study, the
172 corresponding shorelines were derived from this data. The details of the data processing are
173 presented in Appendix A. In addition, a shoreline corresponding to May 2008 (slightly before

the occurrence of Hurricane Ike) was identified on Google Earth and consequently was plotted in the same coordinate system that was used for the post-hurricane historical shorelines. The shoreline in May 2008 acted as a reference for assessing the degree that Galveston beach recovered following Hurricane Ike. Fig. 5a shows the sequence of shorelines between 2008-2016, while Fig. 5b shows the changes relative to May 2008, (by subtracting the ordinates $y_{i,2008}$ of the 2008 shoreline from the corresponding ordinates of the shorelines in the years between 2010-2016, where i=1,2,… is the enumeration of grid points on the X' axis). Where changes are negative the beach is still revering from its 2008 position, while where changes are positive the beach has more than recovered.

Fig. 5.

Fig. 5a illustrates a conspicuous accumulation of sediment material along the entire beach, from 2010 to 2014. Fig. 5b shows that apart from the beach sections on the right hand-side and near South Jetty and Groyne 1, respectively, there is incomplete beach recovery. The area between the accretive zone near South Jetty and Groyne 14 exhibits slower recovery than the rest of the groyne field. This trend is verified from Google Earth images. For example, Fig. 6 shows the shoreline evolution in the second groyne compartment counting from South Jetty, which lies between Groyne 15 and Groyne 14 in Fig. 5, confirming the trend.

Fig. 6.

3. Methodology

A one-line modelling framework was adopted as the beach is shaped strongly by longshore transport, but with alterations made to account for cross-shore removal and addition of

sediment. The One-Line model used here is a shoreline model which is based on the conservation of mass and a longshore sediment transport equation.

The one-line model was first proposed by Pelnard-Considère (1956) in his study of beach behaviour near groynes. In a more formal mathematical treatment Larson et al. (1987) showed that the equation governing the movement of a single height contour could be simplified to a diffusion type process under the assumptions of: constant wave direction; wave crests making small angles with respect to the shoreline trend; small shoreline gradients; and an initially straight shoreline running parallel to the x-axis. The equation may be written as:

$$\frac{\partial y}{\partial t} = \varepsilon \frac{\partial^2 y}{\partial x^2} \quad (1)$$

where t is time, x is the longshore distance on an X axis, y is the shoreline position on a Y' axis perpendicular to the X' axis and ε is a diffusion coefficient given by the equation $\varepsilon=2Q_o/D$. the quantity Qo is the amplitude of longshore sediment transport, and $D=D_C+D_B$, where D_C is the depth of closure and D_B is the berm height. The following extended version of Eq. (1), (e.g. Hanson, 1987), incorporates a source or sink of sediment material:

$$\frac{\partial y}{\partial t} = \varepsilon \frac{\partial^2 y}{\partial x^2} + q_s \quad (2)$$

where $q_s(x,y,t)$ is the sediment transport rate per unit area, coming from a source or a sink ($m^3/m/sec$).

Analytical solutions of Eq. (1) may be found via integral transform techniques for specific boundary conditions (e.g. Larson et al., 1997). Due to the fairly restrictive assumptions made in deriving Eq. (1) the applicability of analytical solutions is limited to idealized cases. Over time, some of these restrictions have been loosened while retaining the benefits of analytical solutions such as accuracy and the absence of numerical instability, (see e.g. Walton and Dean, 2011; Valsamidis and Reeve, 2017). Computational solutions to the One-Line model allow many of the assumptions used in analytical solutions to be lifted. However, they require

time-stepping and may exhibit numerical instability, (e.g. Hanson 1987, 1989). An intermediate approach that lies between analytical and computational approaches is the semi-analytical solution proposed by Reeve (2006), which provides general analytical solutions that can be evaluated through numerical integration. These combine some advantages of both the analytical and the computational solutions; for instance, they can account for time-varying wave conditions, arbitrarily shaped initial shoreline, and are free of numerical instability. Here, we construct a site-specific one-line semi-analytical model to describe the morphodynamic evolution of Galveston beach. Specifically, the semi-analytical solutions for shoreline evolution near a groyne (Reeve, 2006) and for a groyne compartment (Zacharioudaki and Reeve, 2008) were combined in conjunction with suitable internal boundary conditions (BCs), (Valsamidis and Reeve, 2020), to describe the groyne field in Galveston beach, as depicted in Figure 7.

Fig. 7.

The beach from South Jetty westwards to the end of the seawall was represented by 15 groyne compartments plus an open stretch of beach with a single groyne on its lefthand (eastern) end. The semi-analytical model thus consisted of 15 sets of solutions for groyne compartments and one solution for a groyne at the end of an open beach; all linked together to describe the transmission of sediment between adjacent compartments of the model.

The details of the semi-analytical solutions for shoreline evolution in groyne compartments and near a single groyne are presented in Appendix B for ease of reference. These semi-analytical solutions incorporate arbitrary time-varying boundary conditions.

In order to use the semi-analytical solutions to describe the beach movements along Galveston Island beach it is necessary to describe the processes of material travelling through

249 permeable groynes and also by-passing the tips of the groynes in a manner that can be
250 incorporated into the solutions, as illustrated in Figure 8.
251
252 Fig. 8.
253
254 A methodology that permits this is that due to Hanson (1989), who proposed scheme to
255 describe these processes within the framework of a one-line model. The approach is based on
256 the notion that longshore transport occurs across the cross-sectional profile from shoreline out
257 to the depth of closure. Under arbitrary instantaneous wave conditions the seaward extent of
258 longshore transport may not extend as far offshore as the depth of closure. In this case,
259 Hanson (1989) suggested that the depth of active longshore transport, D_{LT}, can be estimated
260 from $D_{LT} = \frac{1.27}{\gamma}(H_{s,b})$ (3)
261 where $H_{s,b}$ is the significant wave at breaking position; and γ is the wave breaking index. D_{LT}
262 varies in time according to the variation of H_{sb}. Let us denote the depth at the tip of the
263 groyne by D_G. Further, approximating the beach by a plane slope the following relationships
264 follow automatically from simple geometrical considerations:
265 $y_{LT} = D_{LT}/sl$ and
266 $y_G = D_G/sl$
267 where sl is the beach slope in the cross-shore direction, y_{LT} and y_G are the distance from the
268 shore of the depth of active longshore transport and the groyne tip respectively. If $y_{LT} < y_G$
269 then no by-passing occurs as the groyne blocks the whole of the section of the profile in
270 which there is longshore transport. Beach material may still permeate through the trunk of the
271 groyne, and the amount is determined by the transport rate and the permeability. If $y_{LT} > y_G$
272 then by-passing can occur in the region of the cross-section profile for which $y_G < y < y_{LT}$. To
273 estimate the amount of by-passing it is assumed that the longshore transport is spread

uniformly across the section of the beach profile for which longshore transport is active. The by-passing rate, Q_{bp} is then simply the potential transport rate scaled by the proportion of the active profile that extends beyond the tip of the groyne:

$$Q_{bp} = Q.(y_{LT} - y_G)/y_{LT}$$

where Q is the sediment transport rate determined from a suitable transport formula. This condition is illustrated in Fig. 9.

Fig. 9.

Now, as the groyne lengths are known, and the beach slope is approximately 1% (as estimated from the bathymetric surveys), the corresponding values of D_G may be computed for every groyne. The sediment transport past each groyne, accounting for permeability and by-passing, can thus be calculated as the sum of the proportion of the longshore transport that by-passes the groyne plus the product of the proportion of the longshore transport that is blocked by the groyne, multiplied by the permeability. In symbols:

$$F=p(1-b) + b \quad (4)$$

where F is the total percentage of sediment flux passing from the one modelled area to the following one, p is the permeability (as a percentage) of the groyne, and b is the percentage of bypassing. The permeability of the groynes was taken to be equal to 30% following the estimates of Frey et al. (2015).

Hourly wave measurements were obtained, from the free online database owned and maintained by the National Buoy Center, for Station 42035 which is located *22 NM* east of Galveston Island, where the water depth is *15.8 m*. The records consist of significant wave height, peak period and mean wave direction. Wave transformations were performed along a

seabed cross-section from the buoy towards Galveston beach via a simple refraction-shoaling calculation which is described by Valsamidis et al. (2013), and is presented in Appendix C. The frequency distribution of waves by direction over the period 2010 to 2015 is shown in Fig. 10, where angles are measured relative to the shore normal. The predominant wave direction would be expected to cause littoral drift towards the South Jetty, as is observed in practice.

Fig. 10.

It remains to determine the potential longshore transport rate. Several formulae are available for this purpose and here we have used the CERC formula (CERC, 1984). The diffusion coefficient ε (see Eq. (1)) according to the CERC formula is given by Eq. (5):

$$\varepsilon = \frac{K g H_{sb}^2 C g_b}{8(S_g - 1)\,\lambda\,(D_c + D_B)} \qquad (5)$$

where K is a nondimensional empirical constant, Cg_b (*m/sec*) is the wave breaking celerity, $Cg_b = \sqrt{gD_b}$, D_b is the wave breaking water depth and a typical value was considered equal to *1m*, S_g is the specific gravity and is a dimensionless quantity which is equal to *2.65*, g is the acceleration of gravity and is equal to 9.81 m/sec^2, D_c is the depth of closure and D_b is the berm height with values equal to D_c=*6.10m* (*20 ft*) and D_b= *1.22 m* (*4 ft*), (Frey et al., 2015). The model was calibrated over the period April 2010 to April 2011. The measured wave sequence from the offshore buoy was transformed to the nearshore to drive the 1-line model. No additional sources of material were introduced in this process and the calibration consisted of varying the parameter K in the range between 0.005 and 0.90. The value giving the best results was K=0.05.

In the absence of additional information we have adopted a simple approach to represent the accretional trend observed in the groyne compartments, between South Jetty and Groyne 1.

That is, material is assumed to be added uniformly across each groyne compartment at a constant rate. Mathematically, this is implemented in Eqs (B1) and (B4) by specifying linear source terms *s(x,t)* for every groyne compartment, corresponding to the *q(t)* calibrating values that are discussed in Section 4. Source terms, *s(x,t)*, are given in *m/week*, by the following Eq. (6):

$$s = \frac{q_s}{(D_c + D_B)} \tag{6}$$

As the accretion in the first groyne compartment (between South Jetty and Groyne 15) is strongly weighted towards the South Jetty side the uniform distribution in this compartment was modified through an additional term of the form *-(1-x/L)* . In Table 1, the finite Fourier cosine transformations that were used are summarized:

Original function	**Transformed via finite Fourier cosines**
1	*2* if $\psi=0$ or *0* if $\psi=1,2,3\ldots$
-(1-x/L)	$-[\frac{1}{2} + \frac{4}{\pi^2}\cos\left(\frac{\pi\psi}{L}\right) + \frac{1}{9}\cos\left(\frac{3\pi\psi}{L}\right) + \frac{1}{25}\cos\left(\frac{5\pi\psi}{L}\right) + \cdots]$

Table 1: The functions which were used for the description of the *s(x,t)* function, and their finite Fourier cosine transformations.

The total source sediment discharge rate in the first groyne compartment between South Jetty and Groyne 15 was distributed in a proportion 80% to 20%. Specifically, the transformed source terms became, for $\psi=0$:

$$\hat{s}(\psi, w) = a * 2 - \beta * \left[\frac{1}{2} + \frac{4}{\pi^2}\cos\left(\frac{\pi\psi}{L}\right) + \frac{1}{9}\cos\left(\frac{3\pi\psi}{L}\right) + \frac{1}{25}\cos\left(\frac{5\pi\psi}{L}\right) + \cdots\right] \tag{7}$$

while, for $\psi=1,2,3\ldots$:

$$\hat{s}(\psi, w) = -\beta * \left[\frac{1}{2} + \frac{4}{\pi^2}\cos\left(\frac{\pi\psi}{L}\right) + \frac{1}{9}\cos\left(\frac{3\pi\psi}{L}\right) + \frac{1}{25}\cos\left(\frac{5\pi\psi}{L}\right) + \cdots\right] \tag{8}$$

where α (=0.8) corresponds to the weighting of the uniform source term along the groyne compartment and β (=0.2) corresponds to the weighting of the additional source term close to South Jetty.

The term appearing in Eq. (B1), $\hat{s}(0, w) = \int_0^a s(x, w)dx$, simplifies as follows:

345 $$\hat{s}(0,w) = \int_0^a a * 1 * s - \beta * s * (1 - \frac{x}{L})dx \Rightarrow \hat{s}(0,w) = a * s * L - \beta * s * \left[x - \frac{x^2}{2L}\right]_0^L$$

346 $$\Rightarrow \hat{s}(0,w) = \left(a - \frac{\beta}{2}\right) * s * L \quad (9)$$

347 Corresponding expressions were used for the uniform sources in the remaining groyne
348 compartments.

349 Solutions were computed at intervals of 1 week to provide a reasonable temporal resolution.
350 A grid of 764 points was used to represent the longshore domain. The calculations took
351 approximately 30 minutes to determine solutions over the period April 2010 – April 2011 on
352 a computer with an Intel(R) Core (TM) i7-7600U CPU 2.8 GHz processor and 16 GB RAM.

353

354 **4. Results**

355 The calibrated model results are shown in Fig. 11, for the case of no sediment source terms. It
356 is clear that the conspicuous trend of accretion, which is more apparent along the first groyne
357 compartment between the South Jetty and Groyne 15, but also occurs to a lesser degree in the
358 other groyne compartments, is not captured by just longshore transport alone.

359

360 Fig. 11.

361

362 The Root Mean Square Error (RMSE) was relatively high in this case and equal to *20.6m*.
363 The discrepancy clearly lies in an underestimation of the total sediment volume on the beach.
364 The underprediction of sediment volume suggests that a source of sediment supply has been
365 omitted in the modelling process.
366 The surveys showed a generally accretive trend along Galveston beach from 2010 to 2014,
367 while from 2014 to 2016 the shorefront was fairly stable. The observed accretive trend from
368 2010 to 2014 is attributed to a natural beach recovery process following the landfall of
369 Hurricane Ike in 2008 close to South Jetty, augmented by dumping of dredgings near South

370 Jetty as mentioned in the Introduction. It is likely that sediments eroded by Hurricane Ike
371 were deposited offshore and have since been gradually moved back to the shore by wave
372 action. The interaction of South Jetty with tidal currents is likely to set up a gyre in residual
373 currents off the tip of South Jetty that would act to accumulate sediments. However, the
374 spatial distribution of the deposits is unknown. By using recent wave observations and the
375 one-line modelling, we can investigate how different patterns of sediment supply match with
376 the observed beach recovery, and thereby infer the likely spatial distribution of the nearshore
377 deposits. These sources are incorporated in the One-Line model in Eq. (2) and correspond to
378 the term q_s that describes a source or sink of sediment.
379 Given this, and the eastward net littoral drift it is unlikely that material was fed solely from a
380 distinct store of material near South Jetty, as this would not spread westwards to nourish the
381 beaches in the groyne field and beyond. An alternative scenario, Scenario 1, is a distinct store
382 offshore of the nodal point. This could feed the beaches to the west of the groyne field and,
383 with sufficient permeability and by-passing, potentially nourish the beaches in the groyne
384 field, as well as creating an accumulation near South Jetty due to its interruption of the
385 longshore drift. The difficulty with this scenario is that there is no obvious geomorphological
386 driver that would provide a mechanism to select the nodal point as the place for preferential
387 deposition resulting from Hurricane Ike. An alternative, Scenario 2, would have a distinct
388 store near South Jetty, plus a diffuse store running the length of the remainder of the beach in
389 the form of an offshore shore-parallel sand bar. This would correspond to the situation in the
390 first scenario plus a uniform removal of sediment by Hurricane Ike and subsequent gradual
391 feeding of the shoreline.
392 Scenario 1:
393 In this scenario a single large supply of sediment material is created on the western side of
394 the groyne field to investigate whether this could produce the observed accretion within the

395 groyne field up to the South Jetty, relying on the predominant littoral drift. A sediment source
396 was modelled on the western side of the groyne field such that the beach was supplied with
397 an equal amount of sediment material (integrated over time and length of the source) with the
398 one which was applied in the groyne compartment between the South Jetty and Groyne 15 in
399 Scenario 2 (see Fig.14). The simulation was performed over the period 2011-2015
400 considering no other sources along the beach. The sediment was supplied uniformly along
401 this beach section at a rate that decreased with time, in a manner identical to that described in
402 Scenario 2 below. As illustrated by the results in Fig.12, sediment is not transported in
403 sufficient quantities through the groyne field towards South Jetty to successfully simulate the
404 observed accretion. Groyne 1 acts effectively to interrupt the longshore transport, resulting in
405 accretion of the beach west of Groyne 1 and very little accretion of the beach within the
406 groyne field or near South Jetty.
407
408 Fig. 12.
409
410 We thus conclude that the recovery of the beach is not due to an isolated supply of sediment
411 to the west of the groyne field and further, it seems that an additional source of sediment is
412 necessary to account for the observed accretion near South Jetty.
413 Scenario 2:
414 In this scenario a sand bank located near South Jetty and a sand bar offshore of Galveston
415 beach are assumed to have been formed as illustrated in Figure 13. The sand bank is located
416 near South Jetty and is hypothesized to have nourished the area between South Jetty and
417 Groyne 15 up to 2014 (Fig. 5). The sand bar is assumed to be located offshore of the groyne
418 field, and to feed the coastal area between Groyne 15 and Groyne 1.
419

Fig. 13.

The form, timing and volume of the sediment supply is unknown, leaving a myriad of possibilities that could be hypothesised. To investigate the impact of different sediment supply on the beach evolution several sub-scenarios were envisioned. To this end, linear sources of sediment were specified, causing accretion uniformly within in every groyne compartment of the groyne field, from the South Jetty to Groyne 1. Furthermore, from Fig. 5 it can be intimated that the accretion rate in the first groyne compartment, between South Jetty and Groyne 15, is not constant but rather decreases over time; specifically, the observed accretion rate in 2010-2011 is greater than the corresponding one in 2011-2015, while after 2014 it is almost diminished. To mimic this behaviour, for the first groyne compartment only, a decreasing rate of sediment flux was considered with an exponential form $AExp\{-Bt + C\}$. The constants A, B and C were varied systematically to achieve a best fit for the period 2010 to 2011. The form shown in Fig.14 provided the closest recreation of the observed shoreline change. Also shown are the maximum and minimum sediment fluxes that were used in the fitting process.

Fig. 14.

It is clear from Fig. 14 that while a supply to the first groyne compartment can improve the prediction of the observed beach position in this area, it has little impact on the beach position in the remaining compartments, indicating that material added at this part of the beach does not travel easily further westwards towards the seawall; a conclusion that would be expected from the prevailing littoral transport direction.

For all remaining groyne compartments, constant rates of sediment flux were applied to mimic the gradual accretion observed in these areas (Fig. 5). Specifically, in the second groyne compartment between Groyne 15 and Groyne 14, q_2 values were tested for the range $1 \leq q_2 \leq 10\ m^3/week$ and the optimum value $q_2 = 2.52\ m^3/week$ found. Regarding the other groyne compartments up to Groyne 1, the following values of sediment flux rate were chosen: $q3 = q4 = \ldots = q14 = 1.08\ m^3/\text{week}$, considering values in the range: $0.5 \leq q_i \leq 5\ m^3/week$, where $i = 3,4 \ldots 14$. Results from the semi-analytical model for the best-fit case are presented in Fig.15.

Fig. 15.

The Root Mean Square Error (RMSE) corresponding in this fitting process was *RMSE=13.85m*.

The above process does not constitute a formal optimization procedure but provides a systematic approach to optimize the simulation results with the assumed form of sediment source distribution. As a check on the assumed source distribution, with the best case scenario distribution of sources found above, the model was 'validated' over the time period April 2011 – May 2015. The results are shown in Fig. 16 and the corresponding *RMSE* was *16.13m*.

Fig. 16.

The error in this case, over a four year prediction period, is slightly larger than for the optimization performed over a one year period, but suggests the hypothesized source distribution is a plausible one.

5. Discussion

The accretive trend along Galveston beach which is shown in Figures 5a&b and 6, over the period 2010 to 2014, followed the significant beach loss caused by Hurricane Ike in 2008 (Fig. 4). As mentioned in Section 2 this area has a limited amount of sediment supply so the arrival of sediment to the extent shown by the historical surveys over the period 2010 to 2016 is quite remarkable. The recovery period of Galveston beach and dune systems after a major event like a hurricane has been estimated by Morton et al. (1994) to be approximately 5 years. The observed timescale of accretion occurring from 2010 up to 2014 (Figs.5a&b) along Galveston beach agrees well with this.

In addition, as is evident from Fig. 5a&b, there is a larger amount of accretion occurring near the South Jetty in comparison with the rest of the beach. This may be due to the fact that as Hurricane Ike passed over Galveston Bay (Doran et al., 2009; Rego and Li, 2010; Hawkes and Horton, 2012), sediment material moved offshore from Galveston beach, (Sherman et al., 2013), but also through the inlet of Bolivar Roads and towards the offshore tip of South Jetty, (Goff et al., 2010). Subsequently, waves could have transported the sediment material which had earlier been deposited near the tip of the South Jetty back to the eastern part of Galveston beach. The rate at which this process takes place in the first groyne compartment between the South Jetty and Groyne 15, decreases in time (Figs. 5a&b), suggesting that the accretion phenomenon in the first groyne compartment had started earlier than 2010, possibly, almost straight after the passage of Hurricane Ike in 2008. A similar morphodynamic mechanism can be envisaged when the dredgings from the Bolivar Road channel is deposited offshore of South Jetty, forming a sand bank in that area. Then, due to wave action, material is redistributed in the vicinity of South Jetty, reducing the volume in the sand bank, as suggested by Frey et al. (2015).

Moreover, accretion occurs in the region extending from Groyne 15 to Groyne 1 (Figs. 5a&b); between 2010 and 2014. Thus, it could be hypothesized that while the first groyne compartment (extending from South Jetty to Groyne 15) is gradually filled with sand, sediment material is moved along to the other groyne compartments through littoral transport, permeability of the groynes and by-passing. However, this is most unlikely because the prevailing wave conditions in the vicinity of the groyne field (Fig. 10) cause a littoral drift from the end of the groyne field towards the South Jetty.

As an alternative, it was hypothesised the existence of a sand bar offshore of the groyne field. This sand bar is considered to have been formed due to offshore deposits of material that are gradually brought onshore after the hurricane.

Regarding the significant accretion which is observed on the right-hand side of Groyne 1 in June 2016 (Figs. 5a&b), this is due to the nourishment efforts that were executed westwards of the groyne field in 2015. Specifically, in March 2015 a beach nourishment was placed at Dellapena Park, on the west side of the seawall (Guillen, 2017). Moreover, in November 2015 nourishment works were conducted west of 61st Street, (the area west and in the immediate vicinity of Groyne 1, Guillen (2017)).

Some caveats are worth noting in regard to the simple modelling framework adopted here. Firstly, the nearshore wave transformation was simplified by treating the bathymetric contours as being approximately parallel to the shore. This cannot fully describe the effects of the complex bathymetry near Galveston beach on local wave refraction and diffraction effects. Secondly, the sediment transport and response of the beach morphology is modelled within the framework of a one line model, with the well-known associated restrictions on detailed process description. In addition, the semi-analytical beach model does not include spatial variation of breaking wave angle, and so cannot reproduce the effects of wave diffraction on sediment movement. Another limitation of the current modelling work is that it

520 treats only a single sediment fraction, in this case sand. The implications of this are that in
521 parts of the case-study where a significant portion of the beach sediment material is not sand,
522 e.g. near South Jetty where dredged material from the Trinity delta (Fig. 2), which is
523 predominantly muddy (Davis, 2017), is placed at the offshore tip of the South Jetty, results
524 may be less reliable. The discrepancies in shoreline prediction close to South Jetty (Fig. 15
525 and Fig. 16) may be caused by the simplification of wave conditions or variations in sediment
526 composition. A detailed analysis of these issues is not the purpose of this paper but may be
527 investigated further in future research.
528 Fig. 5b shows that beach recovery is not full along the shorefront, although in the part of the
529 groyne field between Groyne 15 and Groyne 1, it occurs to a greater degree than in the first
530 groyne compartment, especially on the left hand-side of Groyne 15, and in its vicinity. From
531 Fig. 5a, the historical shorelines appear to be converging towards to a new configuration
532 along the groyne field, up to 2016. This new beach shape is far away from the shoreline in
533 2008, so it seems that either some sediment material was permanently lost beyond the depth
534 of closure due to Hurricane Ike, or, the recovery is still ongoing at this stage.
535 The semi analytical model is quite general in its applicability and is not restricted to
536 Galveston Island. Indeed, it could be applied, for instance, to Fire Island in New York where
537 Hurricane Sandy made a landfall in 2012 and which has been the subject of several
538 geomorphic and modelling studies, (Goff et al., 2015; Warner et al., 2017; Bennett et al.,
539 2018), and Pea Island Breach located in the Outer Banks of North Carolina, USA, where
540 Hurricane Irene and Hurricane Sandy made landfall in 2011 and 2012, respectively (Montoya
541 et al., 2018).
542

543 **Conclusions**

A unique set of shoreline surveys has provided the basis for an exploration of the recovery of Galveston beach after the passage of Hurricane Ike. These, combined with a semi-analytical one-line model have been used to gain insights into the meso-scale recovery process. An explanation of the morphodynamic evolution of a section of Galveston beach near the city of Galveston, extending from South Jetty up to a point along the Seawall approximately 17 km westwards, has been proposed as a result.

The surveys showed a generally accretive trend along Galveston beach from 2010 to 2014, while from 2014 to 2016 the shorefront was fairly stable. The observed accretive trend from 2010 to 2014 was attributed to a beach recovery process following the landfall of Hurricane Ike in 2008 close to South Jetty, which caused extended beach erosion. Given the sediment limited nature of the site the recovery of the beaches is remarkable and is likely due to material moved and stored in offshore deposits gradually being reworked to the beaches. There are no bathymetric surveys to confirm or refute the existence of such deposits. However, their existence can be inferred from the observed beach recovery and modelling of the beach evolution.

A semi-analytical beach model based on the one-line framework was used to investigate the beach recovery process. Using local wave conditions covering the period 2010-2015 we have established that:

1) It is most unlikely that the beach recovery arose solely through a source of sediment to the beach west of the groyne field, even though the predominant littoral drift at this location is predominantly towards the east. The groyne field, although permeable does not allow sufficient quantities of sand to be transported along the beach to match the speed of beach recovery;

2) A single source of material to the beach near South Jetty does not nourish the groyne compartments or the beach to the west of the groyne field due to the prevailing littoral drift to the east;
3) The combination of a single source in the compartment nearest South Jetty, with a spatial weighting towards the jetty, and a distributed set of smaller sources along the length of the beach provides a better fit to the observations.

Further, we conclude that:

1) Notwithstanding its rather simple description of sediment transport dynamics the One-Line model provides a useful tool for analysing the medium scale evolution and response of beaches;
2) The version of the one-line model used here is based on analytical solutions for basic building blocks of solutions for single groynes and groyne compartments, linked together using time-varying boundary conditions that can account for the permeability of the groynes and by-passing of the tips of the groynes. This modelling approach has been shown to be feasible for an extended length of coast with multiple barriers to littoral drift and arbitrary sources of sediment;

Acknowledgements

AV and DER acknowledge the support of the UK Engineering and Physical Sciences Research Council (EPSRC) through the MORPHINE project (grant EP/N007379/1).

Data access

The shorelines in 2010 and 2011 were created using data sets from the University of Texas Austin's Bureau of Economic Geology in the Jackson School of Geosciences. Moreover, the

Galveston Park Board provided bathymetric data with respect to years 2014, 2015 and 2016. All bathymetric data used in this study is available from Dr Jens Figlus [figlusj@tamu.edu].

Modelling

The new semi-analytical model has been written as a MATLAB code called AMMOS. The code is available from Dr Valsamidis/Prof Reeve on request. [antonios.valsamidis@swansea.ac.uk / d.e.reeve@swansea.ac.uk].

Appendix A. Bathymetric data processing to extract historical shorelines

The 2010 & 2011 shoreline data were provided in a GIS database (drawing shp & dbf file) and a coordinate transformation was made (UTM zone 15 to LM projection) in order to be compatible with the rest of the shoreline data (2014-2016).

The 2014, 2015 & 2016 shoreline data, were provided in an Autodesk Civil 3D drawing file, derived from the DTMs produced from the original field data measurements, and converted from feet to metres.

All shoreline data (coordinates) refer to the NAD83 Texas State Planes, South Central Zone(TX83-SC) coordinate system, using an LM projection and the NAD 83 Datum (horizontal) and to the north America vertical datum of 1988 (NAVD88), and they were plotted in a single drawing (dwg) file.

An A-B axis was drawn, (the total length is 16875 metres), along the average shoreline direction, as a reference.

The A-B (east to west direction) axis has an original azimuth of *257.6087 grads* and was rotated clockwise along with the shoreline polyline data.

The A basepoint coordinates were $X=1015098.0079$ and $Y=4173543.9111$ metres and the clockwise rotation angle was *42.3913 grads*, in order to coincide with the X axis.

The resulting constant *Y* value of the rotated *X* axis was *4173543.9111* metres.

The shoreline deviation from the rotated A-B axis is the shoreline position relative to the A-B axis. That is, the 'y' value shown in Cartesian plots of the beach.

For ease of reference, the rotated data were transposed to the origin of the Cartesian system and the shoreline data (*Y*-Axis) were re-sampled at fixed intervals along the *X*-Axis of *12.5m*. This resolution was sufficient to capture the main morphological features of the beach while avoiding undue computing demands for the semi-analytical modelling.

Appendix B. Semi-analytical solutions - summary

The shoreline evolution in a groyne compartment (Zacharioudaki and Reeve, 2008) is described by a solution to Eq. (2), which is derived via finite Fourier cosine transforms. This solution consists of the sum of the following 4 terms:

$$y_1^{GC} = \frac{1}{\mathrm{a}}\bar{g}(0) + \frac{1}{\mathrm{a}}\int_0^t \varepsilon(w)(j(w) - k(w) + \hat{s}(0,w))dw \quad \text{(B1)}$$

$$y_2^{GC} = \frac{2}{\mathrm{a}}\sum_{\psi=1}^{+\infty} \cos\left(\frac{\psi\pi x}{\mathrm{a}}\right)\hat{g}(\psi)\exp\left(-\int_0^t \frac{\pi^2\psi^2}{\mathrm{a}^2}\varepsilon(u)du\right) \quad \text{(B2)}$$

$$y_3^{GC} = \frac{2}{\mathrm{a}}\sum_{\psi=1}^{+\infty} cos\left(\frac{\psi\pi x}{\mathrm{a}}\right)\int_0^t \exp\left(-\int_w^t \varepsilon(u)\left(\frac{\psi\pi}{\mathrm{a}}\right)^2 du\right)\left(\varepsilon(u)\left((-1)^{\psi}j(w) - k(w)\right)dw\right. \quad \text{(B3)}$$

$$y_4^{GC} = \frac{2}{\mathrm{a}}\sum_{\psi=1}^{+\infty} cos\left(\frac{\psi\pi x}{\mathrm{a}}\right)\int_0^t \exp\left(-\int_w^t \varepsilon(u)\left(\frac{\psi\pi}{\mathrm{a}}\right)^2 du\right)\hat{s}(\psi,w)dw \quad \text{(B4)}$$

In the above equations *g(x)* corresponds to the initial shoreline position, $\hat{g}(\psi) = \int_0^{\mathrm{a}} g(x)cos\left(\frac{\psi\pi x}{\mathrm{a}}\right)dx$ thus, $\hat{g}(0) = \int_0^{\mathrm{a}} g(x)dx$; $'\mathrm{a}'$ refers to the groyne compartment's length; $\hat{g}(\psi)$ is the finite-Fourier cosine transform of *g(x)*; ψ is an integer transform variable; *j(w)* is the time-varying boundary condition on the left side of the groyne compartment; *k(w)* is the corresponding boundary condition on the right side of the groyne compartment; *w* is a dummy variable of integration running from time *0* to arbitrary time *t*. The integrals with respect to *u* yield a number for a given value of *t* while those with respect to *w* require

numerical evaluation. Finally, the source term appearing in Eq. (6) is given by: $\hat{s}(0,w) = \int_0^a s(x,w)dx$

The term y_2^{GC} incorporates the initial shoreline shape while y_3^{GC} the boundary conditions at the groynes. The source term is described by the fourth term y_4^{GC}. However, the term y_1^{GC} involves the initial shoreline position, the source term and the boundary conditions.

Finally, the shoreline evolution in a groyne compartment is given by the summation of Eqs. (B1)-(B4):

$$y^{GC}=y_1^{GC}+y_2^{GC}+y_3^{GC}+y_4^{GC} \quad \text{(B5)}$$

where *j(w)* and *k(w)* are the boundary conditions on the left-hand side and right-hand side groynes of the groyne compartment, respectively.

Similarly, the shoreline evolution near a groyne may be computed via the following equations (Reeve, 2006):

This solution consists of the following 3 terms:

$$y_1^G = \frac{1}{\pi}\left(\pi \int_0^t \varepsilon(u)du\right)^{-1/2} \int_0^{+\infty} g(\xi)\left[\exp\left(-\frac{(x-\xi)^2}{4\int_0^t \varepsilon(u)du}\right) + \exp\left(-\frac{(x+\xi)^2}{4\int_0^t \varepsilon(u)du}\right)\right]d\xi \quad \text{(B6)}$$

where *g(x)* is the initial shoreline position, and ξ is a dummy variable used in the integration process. In many cases the initial beach is taken as a straight line with *g(x)=0* in which case this term is identically zero. y_1^G describes the contribution of the initial shoreline shape to the consequent evolution;

$$y_2^G = \frac{2}{\pi}\int_0^{+\infty}\left(\int_0^t \exp\left(-\int_w^t [\omega^2 \varepsilon(u)]du\right)\tilde{q}(\omega,w)dw\right)\cos(\omega x)d\omega \quad \text{(B7)}$$

where ω is the transform variable used in the Fourier cosine transform operation, $\tilde{q}$ is the Fourier cosine transformed variable of *q*; the latter parameter describes the sediment flow from a source or sink of sediment discharge, and *w* is a variable related to time. This term corresponds to the impact of a source or sink of sediment discharge on shoreline evolution.

Again, in case that there are no sources or sinks *q(t)* may be considered equal to zero, and the second term is zero as well.

$$y_3^G = \frac{1}{\sqrt{\pi}} \int_0^t \varepsilon(w) j(w) \left(\frac{1}{\sqrt{\pi \int_w^t \varepsilon(u)du}} \exp\left(-\frac{x^2}{4\int_w^t \varepsilon(u)du}\right)\right) dw \quad \text{(B8)}$$

where *j(w)* is the boundary condition at the groyne. The third term y_3^G corresponds to the impact of the combination of wave action and the boundary condition at the groyne on the shoreline evolution.

Finally, the shoreline position is given as the summation of Eqs. (B6), (B7) and (B8):

$$y^G = y_1^G + y_2^G + y_3^G \quad \text{(B9)}$$

Appendix C. The wave transformation process

The procedure for every pair of consecutive spatial steps of the sellected cross-shore profile, starting from its offshore limit, is the following:

1. Calculate the refraction coefficient at the seamost point, (depth d_1), as:

$$K_1 = KH_1 / d_1 \quad \text{(C1)}$$

Here, Hunt's (1959) approximation was used so:

$$KH_1 \approx \sqrt{Y^2 + \frac{Y}{f(Y)}};$$

$$f(Y) = (1 + 0.666666Y + 0.355555Y^2 + 0.160846Y^3 + 0.063210Y^4 + 0.021754Y^5 + 0.006541Y^6);$$

$$Y = \frac{\nu^2 \times d_1}{g};$$

$$\nu = \frac{2\pi}{T};$$

and T is the wave period.

2. Similarly, for the adjacent shoreward point, the refraction coefficient is calculated:

$K_2 = KH_2 / d_2$ where d_2 the water depth at the shoreward point.

3. The wave angle at the shoreward point is calculated:

$\varphi_2 = sin^{-1}(\theta_1)$ (C2)

where: $\theta_1 = K_1/K_2 \times \sin(\varphi_1)$; φ_1: wave angle at the offshore point.

4. The wave height at the shoreward point, H_2, is calculated as:

$$H_2 = H_1 \times \sqrt{\lambda_{r,s}} \quad \text{(C3)}$$

where $\lambda_{r,s}$, is the combined refraction and shoaling coefficient given by the following equation:

5. $$\lambda_{r,s} = \frac{(K_2 \times \cos(\varphi_1) \times (1+2\times \frac{KH_1}{\sinh(2\times KH_1)})}{(K_1 \times \cos(\varphi_2) \times (1+2\times \frac{KH_2}{\sinh(2\times KH_2)})} \quad \text{(C4)}$$

6. Check for breaking. The wave breaking condition which was to set the breaking index $\gamma_{0.78} = H_b/d = 0.78$. In other words, wave heights which were exceeding *78%* of the water depth *d*, were considered to break, and their height was reduced to *0.78 x d*.

References

Anderson, J., Wellner, J. S., 2002. Evaluation of beach nourishment sand resources along the central Texas coast: Report to the General Land Office, Houston, Texas, Rice University, 28 p.

Bennett, V.C.C., Mulligan, R.P., Hapke, C.J., 2018. A numerical model investigation of the impacts of Hurricane Sandy on water level variability in Great South Bay, New York: Journal of Continental Shelf Research, v. 161, p. 1-11.

Bever, A.J., McNinch, J.E., Harris, C.K., 2011. Hydrodynamics and Sediment-Transport in the Nearshore of Poverty Bay 31. Observations of Nearshore Sediment Segregation and Oceanic Storms: Journal of Continental Shelf Research, New Zealand, p. 507−526.

Brown, J.M., Davies, A.G., 2009. Methods for medium-term prediction of the net sediment transport by waves and currents in complex coastal regions: Journal of Continental Shelf Research, v. 29, p. 1502–1514.

710 Corbella, S., Stretch, D., 2012. Shoreline recovery from storms on the east coast of Southern Africa:
711 Natural Hazards and Earth System Science, v. 12(1), p. 11-22.
712 Davies, J. L., 1980. Geographical Variation in Coastal Development: Longman Group Ltd, New
713 York, United States, 212 p.
714 Davis, R.A.Jr., 2017. Sediments of the Gulf of Mexico, in: Ward, C.H. Before the Deepwater Horizon
715 Oil Spill, Habitats and Biota of the Gulf of Mexico, Houston, TX, USA, pp. 165-215.
716 Doran, K.S., Plant, N.G., Stockdon, H.F., Sallenger, A.H, Serafin, K.A., 2009. Hurricane Ike:
717 Observations and Analysis of Coastal Change: Open-File Report 2009-1061, U.S. Geological
718 Survey, Reston, Virginia, 35 p.
719 Dunn D.D., Raines, T.H., 2001. Indications and Potential Sources of Change in Sand Transport in the
720 Brazos River, Texas; Water-Resources Investigations Report 01–4057, U.S. Geological
721 Survey, Austin, Texas, 32 p.
722 Finkl, C. W., Andrews, J. L., Campbell, T. J., Benedet, L., Waters, J. P., 2004. Coupling Geological
723 Concepts with Historical Data Sets in a MIS Framework to Prospect for Beach-Compatible
724 Sands on the Inner Continental Shelf: Experience on the Eastern Texas Gulf Coast 1: Journal
725 of Coastal Research, p. 533–549.Frey, A.E., King, D.B., Munger, S., 2014, Recommendations
726 and Requirements for GenCade Simulations: ERDC/CHL TR-14-6, U.S. Army Engineer
727 Research and Development Center, Vicksburg, Mississippi, 148 p.
728 Flemming, B.W., Davis, R.A. Jr, 1994. Holocene Evolution, Morphodynamics and Sedimentology of
729 the Spiekeroog Barrier Island System (Southern South Sea): Senckenbergiana maritima, v. 24,
730 p. 117-155.
731 Frey, A.E., Morang, A., King, D.B., 2015. Galveston Island, Texas, Sand Management Strategies,
732 Technical Report: ERDC/CHL TR-15-XX, U.S. Army Engineer Research and Development
733 Center, Vicksburg, Mississippi, 192 p.
734 Gibeaut, J., 2011. Changes along the Texas barrier island coast: Presentation presented at the Gulf
735 Coast Ecosystem Restoration Task Force Meeting, Galveston, Texas.
736 Goff, J.A., Allison, M.A., Gulick, S.P.S., 2010. Offshore transport of sediment during cyclonic
737 storms: Hurricane Ike (2008), Texas Gulf Coast, USA: Geology, v. 38 (4), p. 351–354.

738 Goff, J.A., Flood, R.D., Austin, J.A. Jr., Schwab, W.C., Christensen, B., Browne, C.M., Denny, J.F.,
739 Baldwinc, W.E., 2015. The impact of Hurricane Sandy on the shoreface and inner shelf of
740 Fire Island, New York: Large bedform migration but limited erosion: Journal of Continental
741 Shelf Research, v. 98, p. 13-25.
742 Guillen, D., 2017. Galveston's nearly $20 million beach expansion complete, concludes $44 million
743 improvement project: The Bay Area citizen, Houston Chronicle (newspaper), web address:
744 https://www.chron.com/neighborhood/bayarea/news/article/Galveston-s-nearly-20-million-
745 beach-expansion-is-11156705.php
746 Hallermeier, R. J., 1980. A profile zonation for seasonal sand beaches from wave climate: Journal of
747 Coastal Engineering, v. 4, p. 253-277.
748 Hall, G. L.,1976. Sediment transport processes in the nearshore waters adjacent to Galveston Island
749 and Bolivar Peninsula: Ph.D. Thesis, Texas A&M University, College Station, 325 p.
750 Hanson, H., 1987. GENESIS-A generalized shoreline change numerical model for engineering use:
751 Lund, Lund Inst. of Tech/.Univ. of Lund.
752 Hanson, H., 1989. Genesis: A Generalized Shoreline Change Numerical Model: Journal of Coastal
753 Research, v. 5, p. 1-27.
754 Hawkes, A.D., Horton, B.P., 2012. Sedimentary record of storm deposits from Hurricane Ike,
755 Galveston and San Luis Islands, Texas: Geomorphology, v.171-172, p. 180-189.
756 Houser, C., Hapke, C., Hamilton, S., 2008. Controls on coastal dune morphology, shoreline erosion
757 and barrier island response to extreme storms; Geomorphology, v. 100 (3–4), p. 223–240.
758 Houser, C. and Mathew, S., 2011. Alongshore variation in foredune height in response to transport
759 potential and sediment supply: South Padre Island, Texas: Geomorphology, v. 125(1), p. 62-
760 72.
761 Hunt, I.J. 1959. Design of seawalls and breakwaters, Journal of the Waterways and Harbors Division:
762 vol. 85(3), p. 123-152.
763 Jensen, S. G., Aagaard, T., Baldock, T. E., Kroon, A., Hughes, M., 2009. Berm formation and
764 dynamics on a gently sloping beach; the effect of water level and swash overtopping; Earth
765 Surface Processes and Landforms, v. 34(11), p. 1533-1546.

766 Kamphuis, J. W., 1991. Alongshore sediment transport rate: Journal of Waterway, Port, Coastal, and
767 Ocean Engineering, v. 117, p. 624-640.
768 King, D., 2007. Wave and beach processes modeling: Sabine Pass to Galveston Bay, Texas, shoreline
769 erosion feasibility study: Technical Report ERDC/CHL TR-07-6, U.S. Army Engineer
770 Research and Development Center, Vicksburg, Mississippi, 150 p.
771 Kobayashi, N., Jung, H., 2012. Beach Erosion and Recovery: Journal of Waterway, Port, Coastal, and
772 Ocean Engineering, v. 138(6), p. 473-483.
773 Kraus, N.,C., Lin, L., 2002. Coastal Processes Study of San Bernard River Mouth, Texas: Stability
774 and Maintance of Mouth: Technical Report ERDC/CHL TR-02-10, USAE-WES, Coastal and
775 Hydraulics Laboratory, Vicksburg, Mississippi, 76 p.
776 Larson, M., Hanson, H., Kraus, N.C., 1987. Analytical solutions of the one-line model of shoreline
777 change: Technical Report CERC-87-15, USAE-WES, Coastal Engineering Research Center,
778 Vicksburg, Mississippi.
779 Larson, M., Hanson, H., and Kraus, N.C., 1997. Analytical solutions of one-line model for shoreline
780 change near coastal structures: Journal of Waterway Port Coastal and Ocean Engineering, v.
781 123, p. 180-191.
782 Larson, M., Kraus, N. C., 1989. SBEACH: Numerical model for simulating storm-induced beach
783 change- Report 1. Empirical foundation and model development: CERC-89-9, Coastal
784 Engineering Research Center, Department of the Army Corps of Engineers, Washington,
785 D.C., United States, 266 p.
786 Mason, C., 1981. Hydraulics and Stability of Five Texas Inlets: Report No. 81-1, U.S. Army Corps of
787 Engineers Coastal Engineering Research Center, Fort Belvoir, Virginia, 109 p.
788 McLean, R. and Shen, J.-S., 2006. From Foreshore to Foredune: Foredune Development over the Last
789 30 Years at Moruya Beach, New South Wales, Australia: Journal of Coastal Research, v.
790 22(1), p. 28-36.
791 Montoya, L.V., Sciaudone, E.J., Mitasova, H., Overtona, M.F., 2018. Observation and modeling of
792 the evolution of an ephemeral storm-induced inlet: Pea Island Breach, North Carolina, USA:
793 Journal of Contental shelf Research, v. 156, p. 55-69.

794 Morang, A., 2006. North Texas Sediment Budget - Sabine Pass to San Luis Pass: Technical Report
795 No. ERDC/CHL TR-06-17, U.S. Army Corps of Engineers Coastal Engineering Research
796 Center, Vicksburg, Mississippi.
797 Morton, R. A., Paine, J. G., 1985. Beach and vegetation-line changes at Galveston Island, Texas:
798 erosion, deposition, and recovery from Hurricane Alicia: University of Texas, Bureau of
799 Economic Geology Geological Circular, v. 85-5, p. 1-39.
800 Morton, R. A., Paine, J. G., Gibeaut, J. C., 1994. Stages and durations of post-storm beach recovery,
801 southeastern Texas coast, USA: Journal of Coastal Research, p. 884–908.
802 Morton, R.A., Guy, K.K., Hill, H.W., Pascoe, T., 2003. Regional morphological responses to the
803 March 1962 Ash Wednesday storm; Coastal Sediments '03, World Scientific Press and East
804 Meets West Productions, Corpus Christi, Texas.
805 Nielsen, A. F., Lord, D. B., 1993. Subaqueous beach fluctuations on the Australian South-Eastern
806 seaboard: Australasian Conference on Coastal and OceanEngineering, Townsville, Australia,
807 p. 645-650.
808 Paine, J.G., Mathew, S., Caudle, T., 2011. Texas Gulf Shoreline Change Rates through 2007: Final
809 Report Prepared for the General Land Office, Bureau of Economic Geology, School of
810 Geosciences, University of Texas, Austin, 38 p.
811 Paine, J.G., Mathew, S., Caudle, T. 2012. Historical shoreline change through 2007, Texas Gulf
812 Coast: rates, contributing causes, and Holocene context: Gulf Coast Association of Geological
813 Societies Journal, v. 1, p. 13-26.
814 Pelnard-Considère, R., 1956. Essai de théorie de l'évolution des formes de rivage en plages de sables
815 et de gâlets: Societe Hydrotechnique de France, IV'ème Journees de L'Hydraulique Question
816 III, rapport 1, p. 74-1-10.
817 Phillips, M.S., 2018. Wave-driven recovery of sandy beaches following storm erosion, the University
818 of New South Wales, Sydney, Australia, 161 p.
819 Phillips, J. D., Musselman, Z., 2003. The Effect of Dams on Fluvial Sediment Delivery to the Texas
820 Coast: Coastal Sediments ’03, Clearwater Beach, Florida.

Phillips, J. D., Slattery, M. C., Musselman, Z., 2004. Dam-to-delta sediment inputs and storage in the lower trinity river, Texas.: Geomorphology, v. 62(1-2), p. 17–34.

Phillips, M. S., Turner, I. L., Cox , R. J., Splinter, K. D., Harley, M. D., 2015. Will the sand come back? Observations and characteristics of beach recovery: Australasian Coasts & Ports Conference, Auckland, New Zealand.

Reeve, D.E., 2006. Explicit Expression for Beach Response to Non-Stationary Forcing near a Groyne: Journal of Waterway, Port, Coastal, and Ocean Engineering, v. 132, p. 125-132.

Rego, J.L, Li, C., 2010. Storm surge propagation in Galveston Bay during Hurricane Ike: Journal of Marine Systems, v. 82, p. 265-279.

Roelvink, D., Reniers, A., van Dongeren, A., van Thiel de Vries, J., McCall, R., Lescinski, J., 2009. Modelling storm impacts on beaches, dunes and barrier islands. Coastal Engineering, v. 56(11–12), p. 1133-1152.

Sallenger, A. H., 2000. Storm impact scale for barrier islands; Journal of Coastal Research v. 16, p. 890–895.

Sherman D.J., Hales B.U., Potts M.K., Ellis J.T., Liu H, Houser, C., 2013. Impacts of Hurricane Ike on the beaches of the Bolivar Peninsula, TX, USA.; Geomorphology, v. 199, p. 62-81.

Siringan, F. P., Anderson, J. B., 1994. Modern shoreface and inner-shelf storm deposits off the East Texas coast, Gulf of Mexico: Journal of Sedimentary Research, v. B64, p. 99–100.

Short, A. D., Woodroffe, C. D., 2009. The coast of Australia. Cambridge University Press, New York, United States, 304 p.

Valsamidis, A., Cai, Y., Reeve, D.E., 2013. Modelling beach-structure interaction using a Heaviside technique: application and validation: Journal of Coastal Research. 65, 410–415.

Valsamidis, A., Reeve, D.E., 2017. Modelling shoreline evolution in the vicinity of a groyne and a river: Journal of Continental Shelf Research, v. 132, p. 49-57.

Valsamidis, A., Reeve, D.E., 2020. A new approach to analytical modelling of groyne fields: Journal of Continental Shelf Research, v. 211, 104288.

van Lancker, V., Lanckneus, J., Hearn, S., Hoekstra, P., Levoy, F., Miles, J., Moerkerke, G., Monfort, O., Whitehouse, R., 2004. Coastal and nearshore morphology, bedforms and sediment

transport pathways at Teignmouth (UK): Journal of Continental Shelf Research. v. 24, p. 1171–1202.

Wallace, D.J., Anderson, J.B., Fernández, R.A., 2010. Transgressive Ravinement versus Depth of Closure: A Geological Perspective from the Upper Texas Coast: Journal of Coastal Research, v. 26, p. 1057–1067.

Walton, T.L., Jr, Dean, R.G., 2011. Shoreline change at an infinite jetty for wave timeseries: Journal of Continental Shelf Research, v. 31, p. 1474–1480.

Warner, J.C., Schwab, W.C., List, J.H., Safaka, I., Liste, M., Baldwin, W., 2017. Inner-shelf ocean dynamics and seafloor morphologic changes during Hurricane Sandy; Journal of Continental Shelf Research, v. 138, p. 1-18.

White, W.A., Calnan, T.R., Morton, R.A., Kimble, R.S., Littleton, T.G., McGowen, J.H., Nance, H.S., Schmedes, K.E., 1985. Submerged lands of Texas, Galveston-Houston area: sediments, geochemistry, benthic and macroinvertebrates, and associated wetlands: Bureau of Economic Geology, Austin, Texas, 145p.

Williams, S. J., Flocks, J., Jenkins, C., Khalil, S., Moya, J., 2012. Offshore Sediment Character and Sand Resource Assessment of the Northern Gulf of Mexico, Florida to Texas: Journal of Coastal Research, v. 60, p. 30–44.

Zacharioudaki, A., and Reeve, D.E., 2008. Semianalytical Solutions of Shoreline Response to Time-Varying Wave Conditions: Journal of Waterway, Port, Coastal, and Ocean Engineering, v. 134, p. 265-274.

Figure Captions

Fig. 1. Location map of Galveston Island (Source: Google Earth), lying between the South Jetty of Bolivar Roads and San Luis Pass. The city of Galveston on the northeast side of the island is protected by a seawall (denoted by a double orange line) and a groyne field symbolized by short yellow lines along the beach front. Orange arrows denote the direction of 2 different littoral drifts; one heads SW towards the San Luis Pass, and one in the opposite NE direction towards the South Jetty. However, a nodal zone near the western side of Seawall, indicated by a yellow ellipse, is the region of drift divergence.

Fig. 2. Coastal setting of Galveston Island: (a) Location of Galveston Island in the Gulf of Mexico; (b) Brazos River discharges near Free Harbour Entrance, while Upper Trinity River and Lower Trinity River discharge into Lake Livingstone and Trinity Bay, respectively; (c) The area in the vicinity of Galveston Island. (Source: Google Earth)

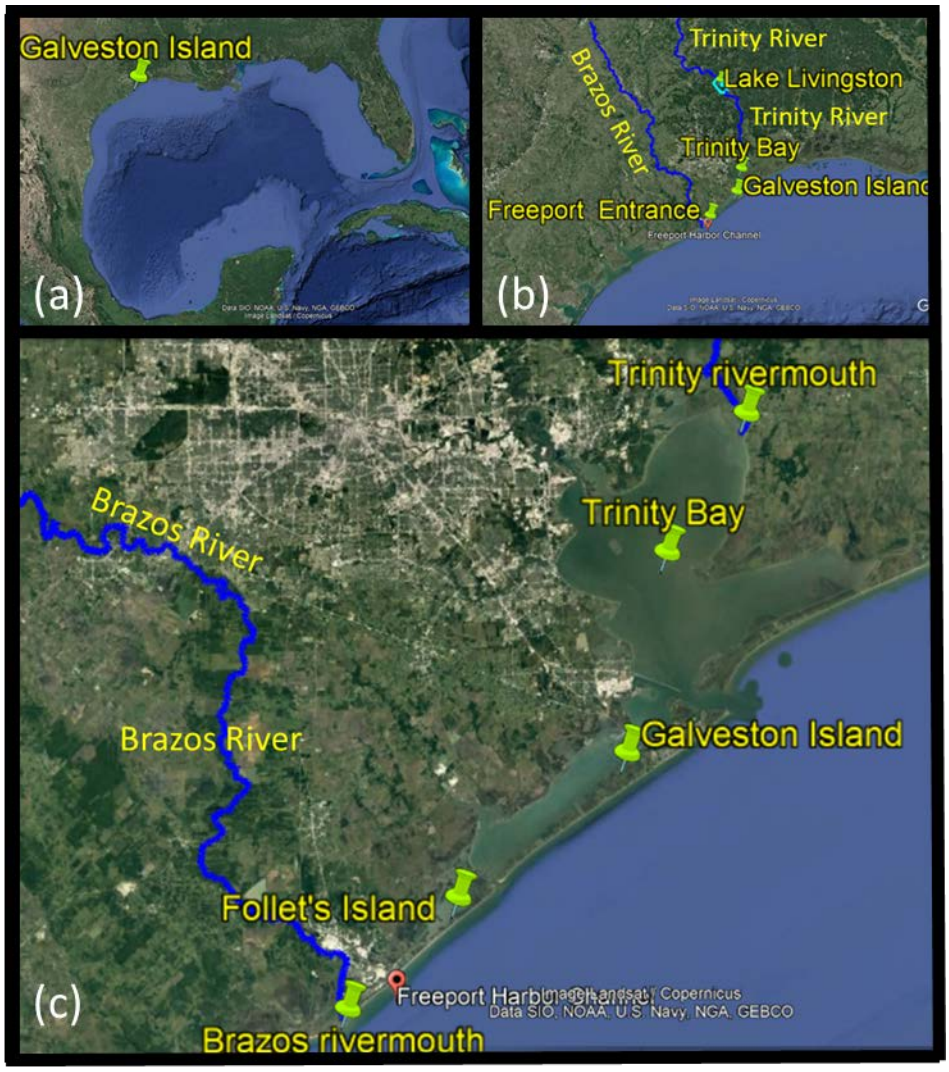

Fig. 3. Hurricane Ike's track as depicted: (a) by Rego and Li (2010), passing over the eastern part of Galveston Island; and (b) by Sherman et al. (2013) considering Hurricane Ike making landfall over Bolivar Peninsula and close to the eastern side of Galveston Island.

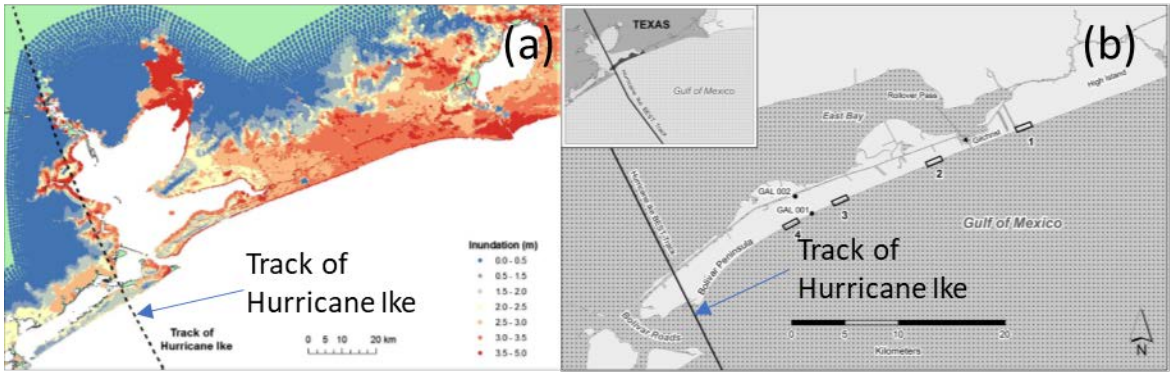

Fig. 4. (from Doran et al., 2009): Photos of the sandy beach and the pier in front of the Galveston seawall on September 10, 2008 (a) and 5 days later (September 15, 2008). The pier structure was destroyed and large volumes of sand from the upper beach section had been eroded during the passage of Hurricane Ike on the 13th of September 2008 (b). Yellow arrows denote reference points used for comparison purposes. Similarly, photos of Galveston beach near the South Jetty on the 10th of September (c) and the 15th of September (d) are compared; here the effects of Hurricane Ike on the beach are more conspicuous.

Fig. 5. (a) Surveyed historical shoreline positions on Galveston Island. The black vertical lines show groyne locations. 15 groynes in total have been constructed and they are enumerated from 1 (terminal groyne) up to 15 (the nearest groyne to South Jetty). (b) Relevant shoreline positions for the years 2010, 2011, 2014, 2015 and 2016 have been plotted with respect to the August 2008 shoreline. Negative values show incomplete beach recovery following Hurricane Ike while positive values denote shoreline advance beyond the

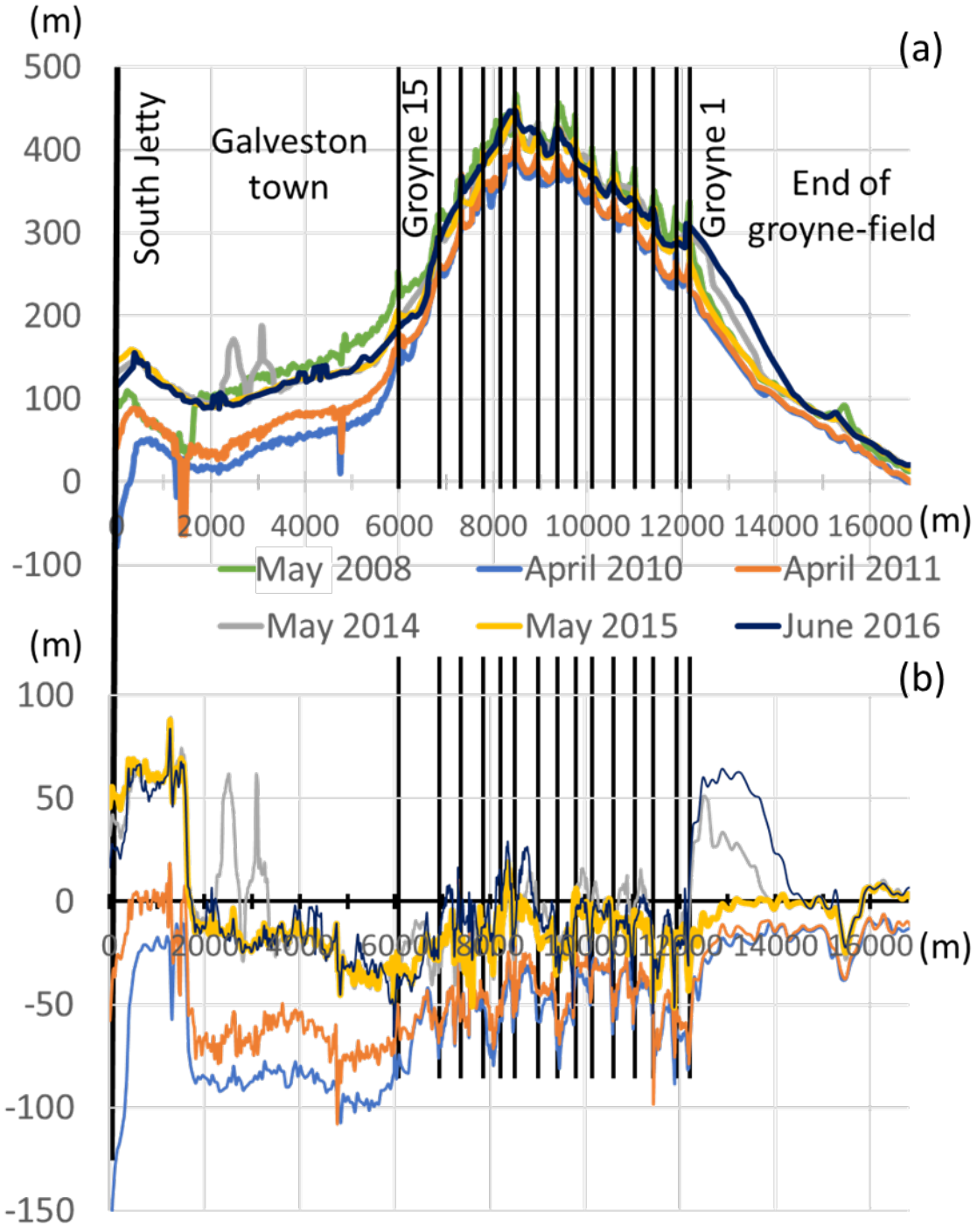

Fig. 6. Shoreline evolution in the 2nd groyne-compartment: the blue line corresponds to April 2010; the orange line to April 2011; the gray line to May 2014; the yellow line to May 2015; and the purple line to June 2016.

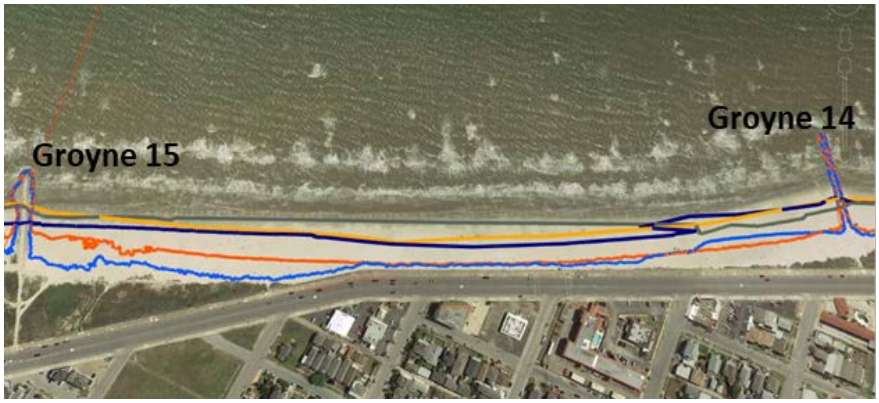

Fig. 7. Schematic illustration of the construction of the beach model for Galveston Island from solutions for groyne compartments and single groynes. The elements are connected using suitable boundary conditions (described in the main text below). The black lines illustrate possible shoreline positions in each area of the domain.

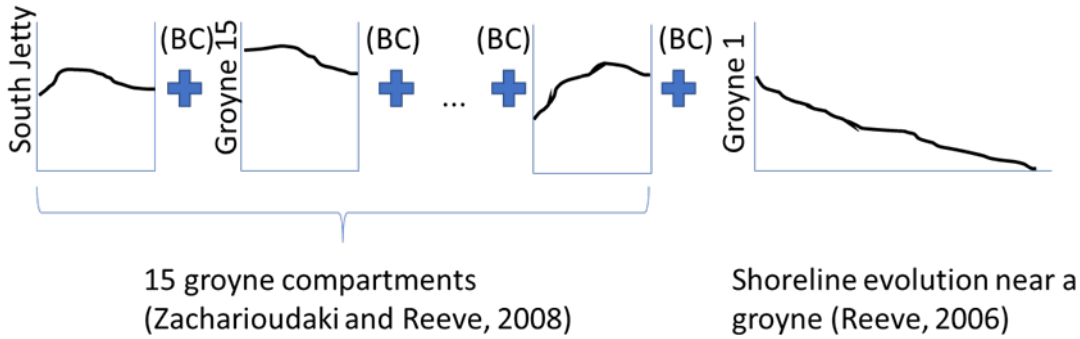

Fig. 8. Simultaneous sediment bypassing of the seaward tip of a groyne and sediment passing through the trunk of a permeable groyne.

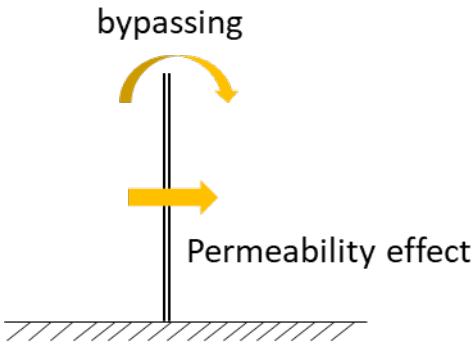

Fig. 9. A wave event *W* causing longshore sediment movement (denoted with the orange arrows) up to the depth of active longshore sediment transport D_{LT}. As $D_{LT}>D_G$, or equivalently $y_{LT}>y_G$, sediment bypassing occurs.

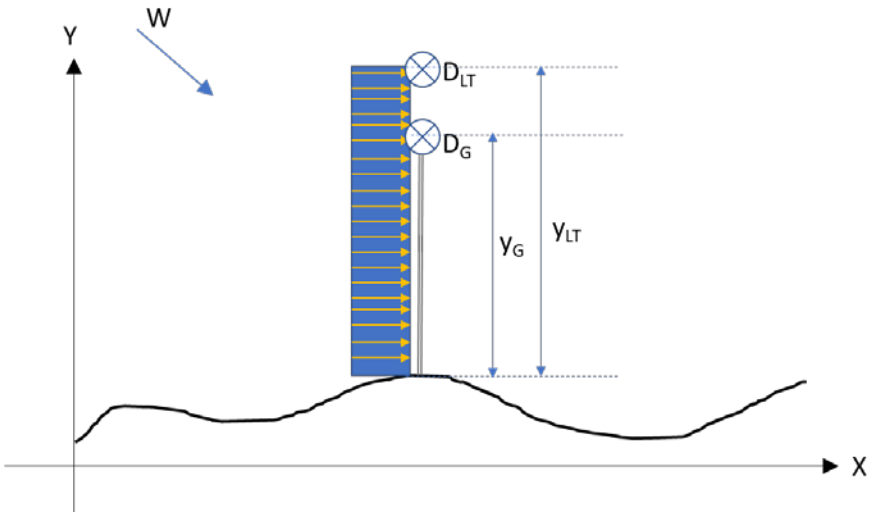

Fig. 10. A rose diagram showing the wave direction distribution over the period 2010 – 2015 for Galveston Island.

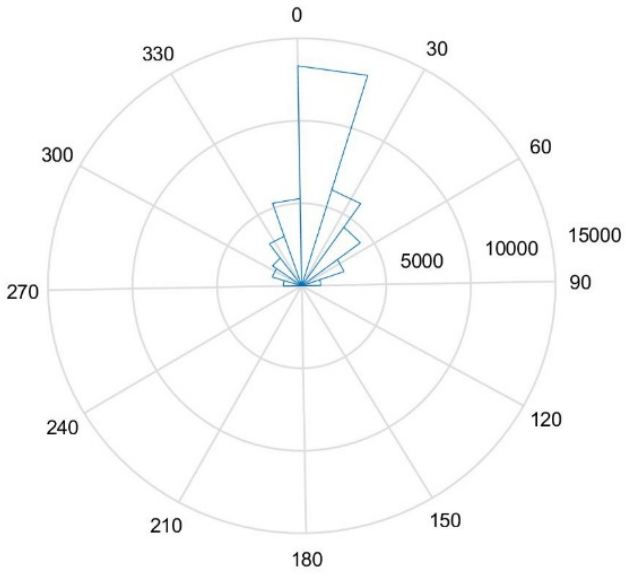

Fig. 11. Calibrated model simulation of Galveston beach over the time period 2010 – 2011. (a) The initial condition is shown in blue, the measured shoreline in April 2011 in orange and the simulated shoreline for April 2011 in grey. (b) The corresponding relative shorelines, considering the reference shoreline in August 2008.

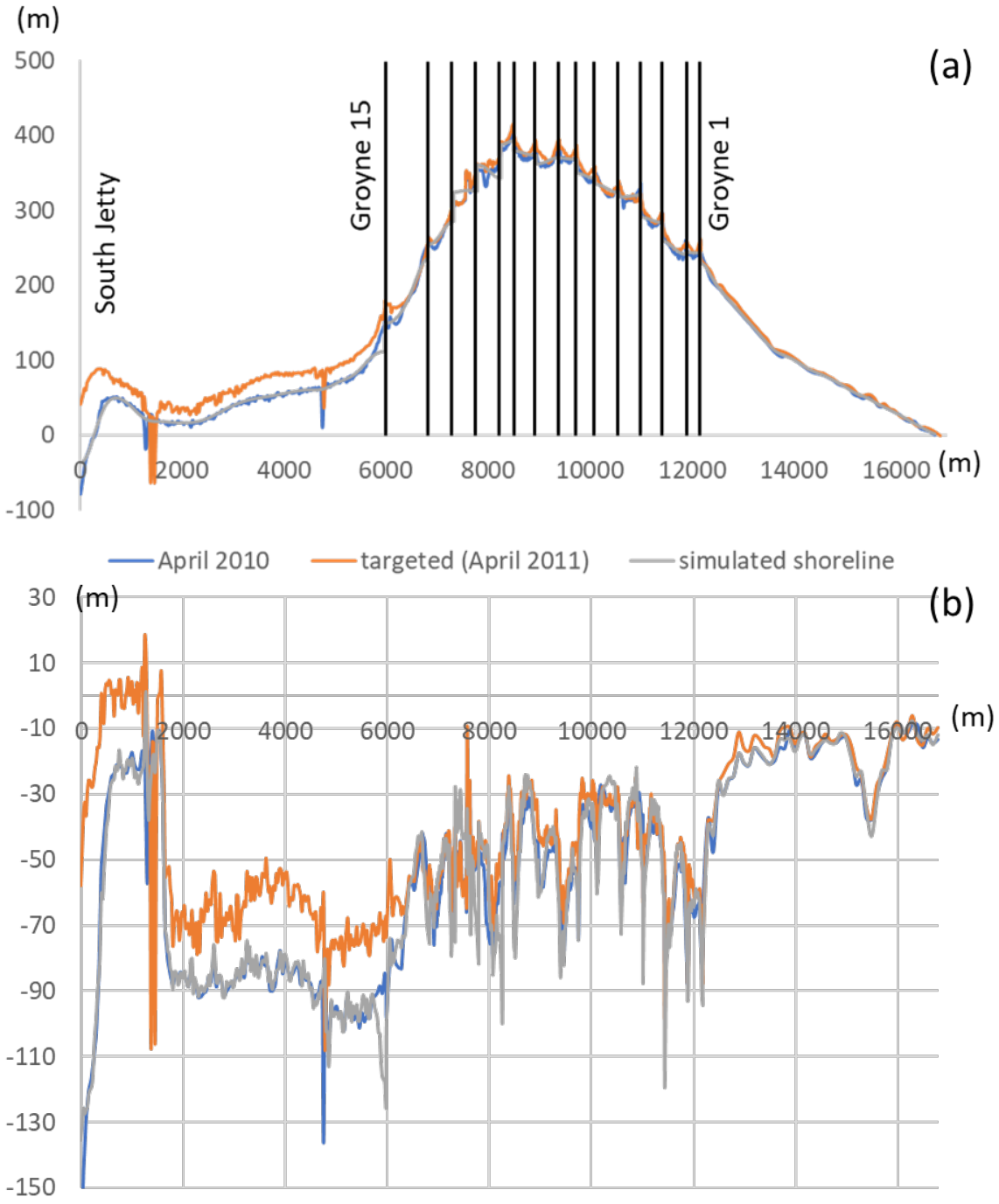

Fig. 12. Results of the simulation of Scenario 1 over the period 2011 to 2015. (a) The blue line represents the initial shoreline position in April 2011, the orange one the targeted shoreline position in April 2015 and the grey line the simulated shoreline in April 2015. (b) The corresponding relative shorelines, considering the reference shoreline in August 2008.

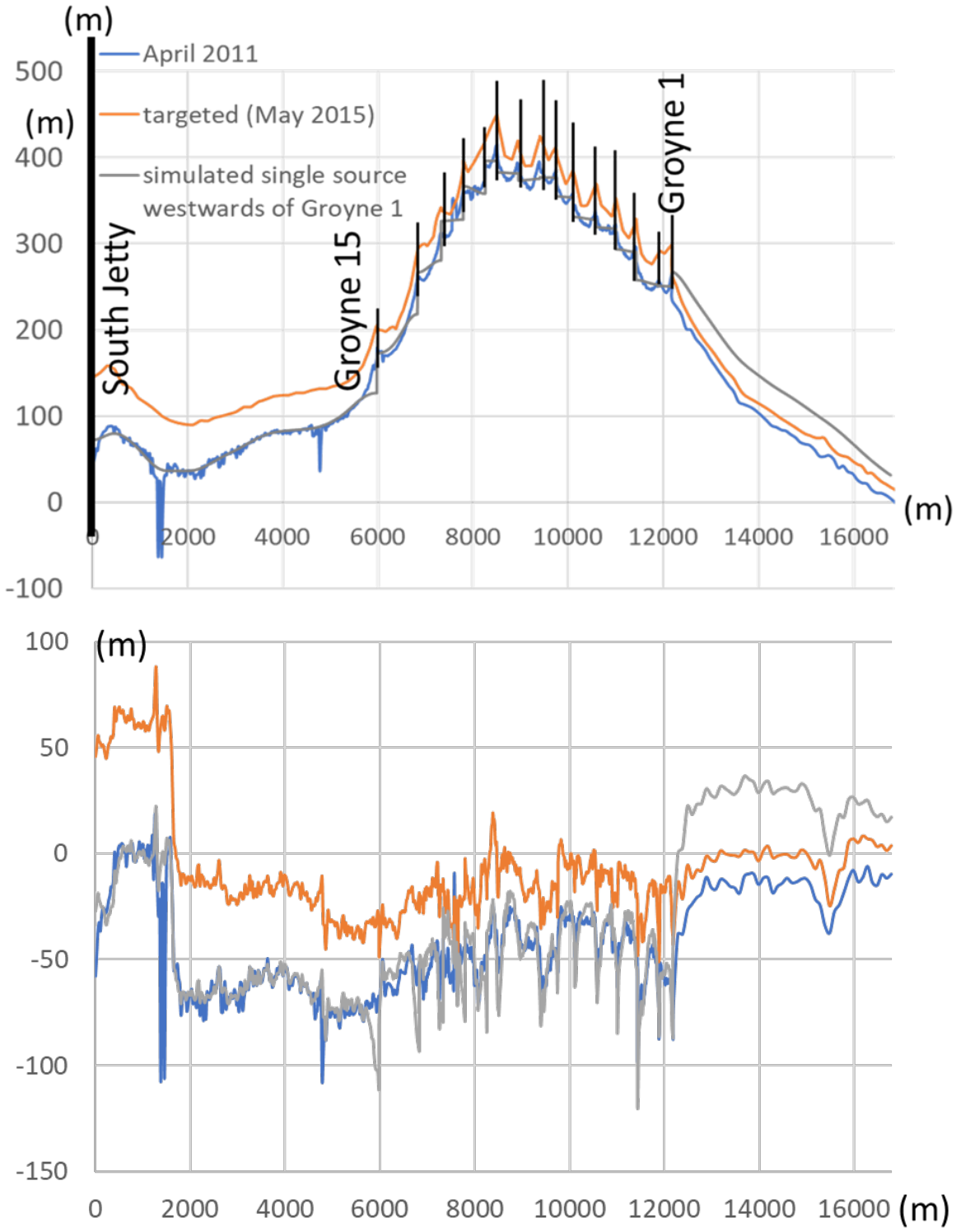

Fig. 13. Distribution of sand sources in Scenario 2 where a sand bank nourishes the area between South Jetty and Groyne 15 and a sand bar nourishes the beach along the groyne field. The yellow thick bars denote the locations of groynes.

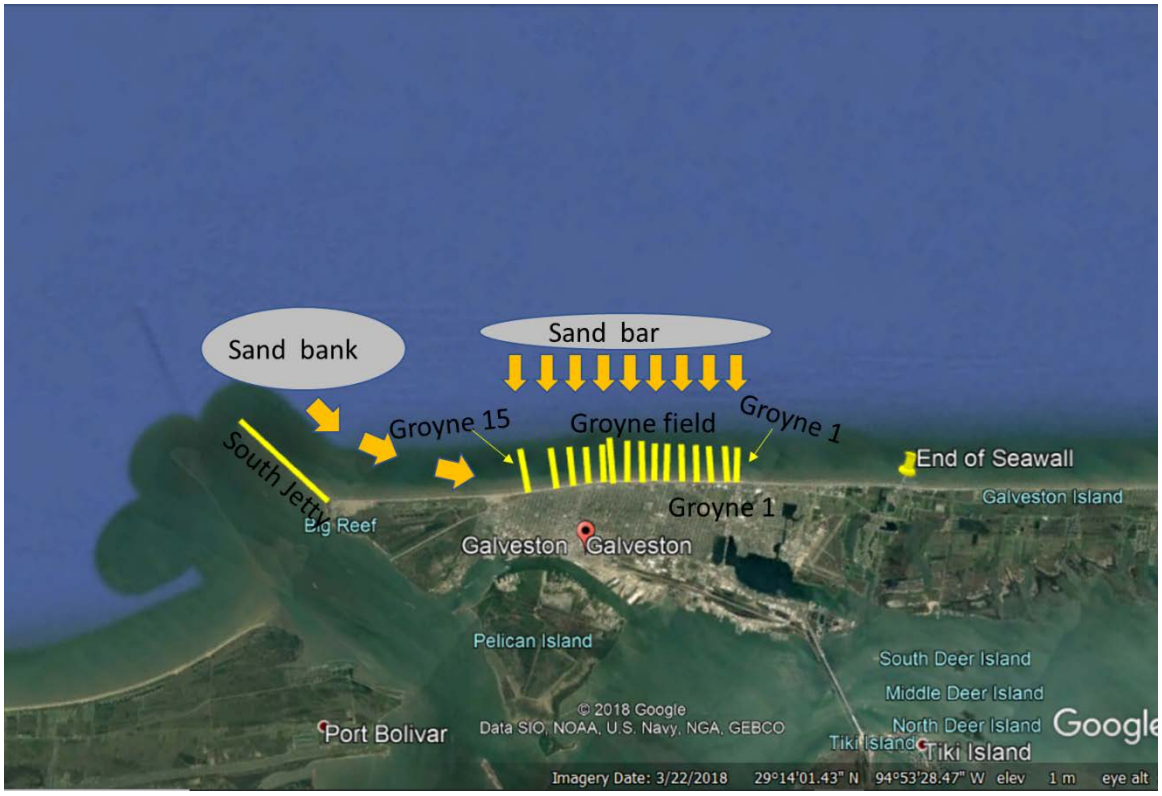

Fig. 14. (a) A decreasing rate of sediment flux q_1 coming from a linear source of sediment material, was considered in the first groyne compartment between South Jetty and Groyne 15. Different time series of sediment flux were tested in the range between q_{min} and q_{max}; (b) The corresponding shoreline positions for q_{min}, q_{max} and q_1 produced RMSE values of *28.77m*, *26.85m* and *20.66m*, respectively.

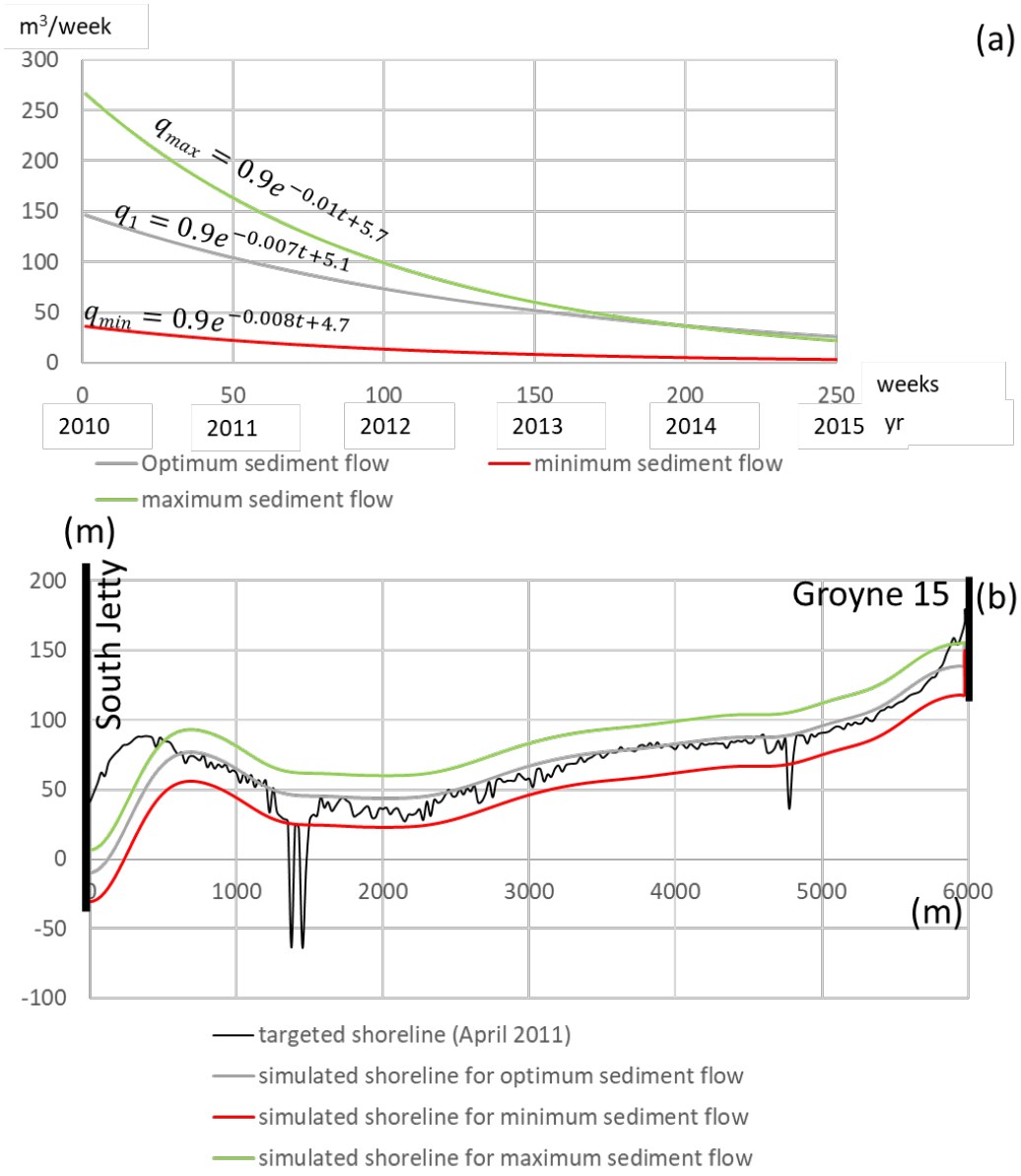

Fig. 15. Best case Scenario 2 solution for the time period: April 2010 – April 2011. (a) The blue line represents the initial shoreline position in April 2010, the orange one the targeted shoreline position in April 2011 and the grey line the simulated shoreline in April 2011. (b) The corresponding relative shorelines, considering the reference shoreline in August 2008.

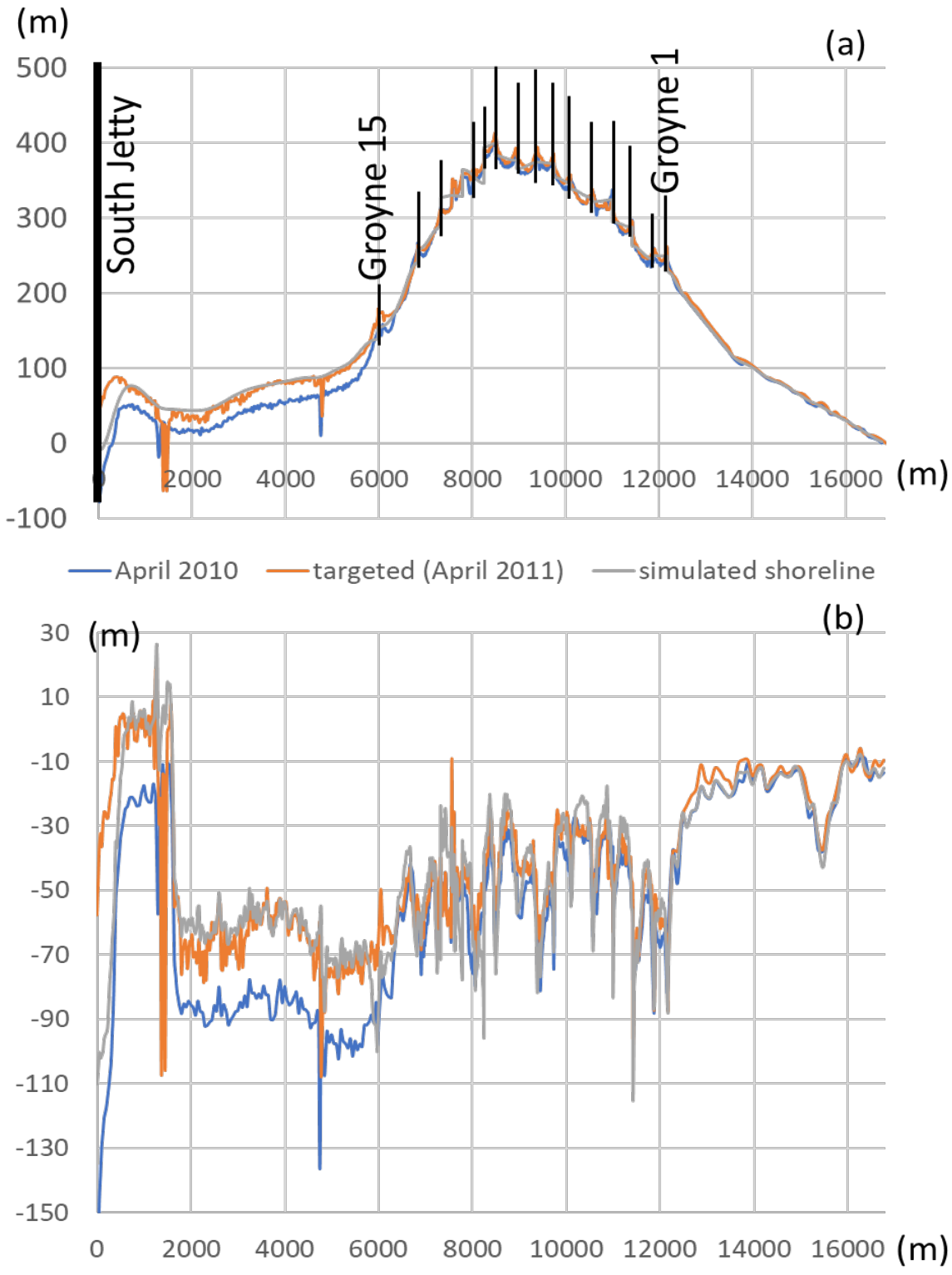

Fig. 16. Validation of the semi-analytical solution in the time period: April 2011 – May 2015. (a) The blue line represents the initial shoreline position in April 2011, the orange one the targeted shoreline position in April 2015 and the gray line the simulated shoreline in May 2015. (b) The corresponding relative shorelines, considering the reference shoreline in August 2008.